Coded Excitation System for Improving the Penetration of Real-Time Phased-Array Imaging Systems

Matthew O'Donnell, *Senior Member, IEEE*

***Abstract*—Based on an analysis of the inherent signal-to-noise ratio (SNR) in medical ultrasound imaging, SNR improvements of 15–20 dB are theoretically possible for real-time phased-array imagers using coded excitation. In this report a very simple coded excitation system for phased arrays based on the principles of "pseudochirp" excitation and equalization filtering is described. This system is capable of SNR improvements of about 15 dB with range sidelobe levels acceptable for many medical imaging applications. Such improvements permit increased operating frequencies, and hence enhanced spatial resolution, for real-time array imagers. Both simulations and measurements are used to demonstrate the efficacy of the method.**

I. Introduction

IN CONVENTIONAL medical ultrasound phased-array systems peak acoustic power, rather than average power, limits the signal-to-noise ratio (SNR) of real-time images. Peak power is restricted so that instantaneous pressure effects, such as cavitation, are minimized. In contrast, the SNR in continuous wave (CW) and pulsed Doppler measurements is limited by average power levels. Indeed, because the duty factor is very small, the average power delivered by most medical imaging systems, often as much as 100 times below maximum allowed levels, is very small compared to Doppler systems [1]. Consequently, methods greatly increasing the average power without affecting the peak power, such as coded excitation, can improve the SNR of ultrasound imaging systems. Such methods may permit routine operation at higher frequencies, where attenuation is increased, with concomitant improvements in spatial resolution.

In radar systems, coded excitation is a well established technique permitting dramatically improved SNR at modest peak power levels compared to conventional pulsed techniques [2]. These systems operate at very large time-bandwidth products resulting in small range sidelobe levels. Both pseudorandom noise and coherent broadband excitations have been explored as codes for ultrasound imaging [3]–[10]. Results to date, however, have been disappointing due to significant range sidelobes created by the small time-bandwidth codes appropriate for real-time medical imaging. In fact, poor range sidelobe levels related to the restricted time-bandwidth product available, as well as the complexity of the electronics needed to produce coded waveforms for full array imaging systems, have resulted in limited application of coded excitation methods to medical ultrasound. In this paper, we explore coding methods producing acceptable range sidelobe levels even for small time-bandwidth products. These methods are very simple and amenable to implementation on real-time array imaging systems. Before describing the coding approach in Section II, we begin with a discussion of the ultimate limits of ultrasound imaging and estimate potential improvements in SNR possible with proper coding schemes.

Starting from simple definitions of scattering efficiency, the inherent SNR of an ultrasound backscatter measurement in the body can be estimated. The backscatter cross section σ is defined as the ratio of the backscattered power to the incident flux. For a collection of scatterers, the cross section is normalized to the unit volume of scatterers contributing to the power. The index η, called the backscatter coefficient, is a standard measure of the efficiency of a collection of scattering centers, as encountered in ultrasound imaging of soft tissue [11]. The total scattered power associated with a single pixel in an image, therefore, is simply the product of the backscatter coefficient for the tissue being imaged with the integral of the incident flux over the sample volume contributing to an individual pixel in the image:

$$P_s = \eta \int I_0 \, dV$$
$$P_s = \eta L \int I_0 \, dA. \tag{1}$$

In (1), the volume integral has been reduced to the product of the pixel length (i.e., range resolution of the image) with the surface integral of the incident flux at any given range, where the backscatter coefficient is assumed constant over the extent of the beam. The flux integral equals the incident power from the transducer, so the scattered power can be simply written as

$$P_s = \eta L P_0. \tag{2}$$

Exposure limits, however, are not defined in terms of incident power, but rather in terms of peak incident flux. Therefore, evaluating the flux integral in terms of the peak, the total

Manuscript received August 15, 1991; revised November 14, 1991; accepted November 15, 1991.

The author was with Corporate Research and Development Center General Electric Company, P.O. Box 8, Schenectady, NY 12301. He is now with the Electrical Engineering and Computer Science Department, University of Michigan Ann Arbor, MI 48109-2122.

IEEE Log Number 9107538.

scattered power available to a receiving aperture is

$$P_s \eta L \lambda^2 \left[\frac{R^2}{A}\right] I_{\text{peak}} \tag{3}$$

where η is the ultrasound wavelength, R is the range of the pixel, A is the area of the aperture and I_{peak} is the peak flux at range R. If we assume that the imaging system is ideally focused for every pixel in the image, then (3) represents the power output at any given pixel. Expressing the range resolution of the imaging system, L, in terms of the bandwidth, Δf, and the sound velocity, V_s, (3) can be rewritten as

$$P_s = \left[\frac{\pi v_s}{2\Delta f}\right]\left[\frac{\lambda^2 R^2}{A}\right]\eta I_{\text{peak}}. \tag{4}$$

Using (4) for the scattered power, the inherent SNR in a single pixel can be calculated from a knowledge of the system noise. Although there are many possible noise sources in a real system, the fundamental limit is simply Johnson noise (i.e., thermal noise) at room temperature:

$$P_{\text{noise}} = 4kT\Delta f \tag{5}$$

where k is Boltzman's constant and T is about 293° K. Using (4) and (5), the inherent SNR can be written as

$$\text{SNR}_{\text{inh}} = \left[\frac{P_s}{P_{\text{noise}}}\right]$$

$$\text{SNR}_{\text{inh}} = \left[\frac{\pi v_s}{8kT(\Delta f)^2}\right]\left[\frac{\lambda^2 R^2}{A}\right]\eta I_{\text{peak}}. \tag{6}$$

The SNR is linearly dependent on both peak incident flux and scattering efficiency. The second term in brackets is the inverse of the focusing gain of the aperture. This expression can also be evaluated in dB, yielding

$$\text{SNR}_{\text{inh}} = 10\log_{10}\left[\frac{\pi v_s \eta I_{\text{peak}}}{8kT(\Delta f)^2}\right] - 10\log_{10}\left[\frac{A}{\lambda^2 R^2}\right] \tag{7}$$

where the second term is the focusing gain of the aperture. In the rest of this paper, the SNR will always be expressed in dB. Equation (7) is a reasonable description of the inherent SNR of a medical imaging system. Please note that a consistent set of units, preferably MKS, should be used for all parameters in (7) to insure proper evaluation.

To estimate the maximum SNR under several different imaging conditions, the peak incident flux must be defined. According to guidelines for adult cardiac imaging [1], the peak flux (i.e., spatial peak, pulse average) is 1.9 W/mm^2 (190 W/cm^2) and the average peak flux (i.e., spatial peak, temporal average) is 4.3 mW/mm^2 (430 mW/cm2). These values are derated assuming a nominal tissue attenuation of 0.03 dB/(mm-MHz). That is, these limits represent *in situ* peak values. Proper derating, including focusing effects, is discussed in detail later.

The inherent SNR of (7) yields very different results for 2-D imaging based on average versus peak power guidelines. If only average power need be considered, then the maximum flux would be

$$I_{\text{peak}} = 4.3\left[\frac{T_p}{\tau}\right]\text{mW/mm}^2 \tag{8}$$

where T_p is the frame period of the imaging system and τ is the pulse duration. For a conventional 5-MHz imager using a 40% fractional bandwidth with a 30 frame/s display rate, (8) becomes

$$I_{\text{peak}} = 72\ \text{W/mm}^2. \tag{9}$$

This peak flux is nearly a factor of 40 higher than the actual peak flux permitted [1]. In general, there is a factor of 15–20 dB improvement in SNR available through coded excitation if maximum peak and average fluxes are maintained simultaneously. This factor of 15–20 dB sets a limit on the possible SNR improvements possible with coded excitation.

If we assume that a proper coded excitation system can be constructed, then the peak limit of (8) should be used to estimate fundamental limits on SNR in the body. In Table I we list the backscatter coefficient as a function of frequency for heart muscle and blood [12], [13]. Also, we assume an average tissue attenuation of 0.06 dB/(mm-MHz) for adult cardiac imaging. The inherent SNR is reduced as a function of range due to tissue attenuation. The input power, however, can be increased as a function of range so that *in situ* radiation patterns approach peak values. This increase partially overcomes losses due to tissue attenuation (at a value of 0.03 dB/(mm-MHz)) and diffraction. Finally, we assume that the aperture on both transmit and receive is opened using a constant f/number criterion until the full aperture is used. From this range on, the aperture remains fully opened. This means that the focus gain term of (7) for a square aperture becomes

$$\text{Focus Gain} = 10\log_{10}\left[\frac{1}{\lambda^2(\text{f/num})^2}\right] \equiv FG_0$$

$$\text{for } R < R_{\text{turn-on}}$$

$$\text{Focus Gain} = FG_0 - 20\log_{10}\left[\frac{R}{R_{\text{turn-on}}}\right]$$

$$\text{for } R \geq R_{\text{turn-on}}. \tag{10}$$

Consequently, the final SNR, including the effects of focusing, tissue attenuation and derating, as a function of range becomes

$$\text{SNR}(R) = \text{SNR}_{\text{inh}}(0) - (\text{Focal Gain}) + (\text{Derating}) - (\text{Tissue Atten.})$$

$$\text{SNR}(R) = \text{SNR}_{\text{inh}}(0) + 20\log_{10}\left[\frac{R}{R_{\text{turn-on}}}\right] + 0.03[2Rf] - 0.06[2Rf] \tag{11}$$

where SNR_{inh} (0)is the inherent SNR at zero range, given by

$$\text{SNR}_{\text{inh}}(0) = 10\log 10\left[\frac{\pi v_s \eta I_{\text{peak}}}{8kT(\Delta f)^2}\right] - FG_0. \tag{12}$$

Equations (10)–(12) are all that is needed to compute the SNR as a function of range for a given imaging configuration if the acoustic flux at the surface of the transducer can reach an arbitrarily high value. In practice, the transducer surface flux also must be below the guidelines given previously. The

TABLE I
VALUES OF BACKSCATTER COEFFICIENT USED IN CALCULATION OF INHERENT SNR.

Frequency (MHz)	η (mm^{-1}) Heart Tissue	η (mm^{-1}) Blood
2.5	4.3×10^{-5}	0.5×10^{-6}
3.75	1.5×10^{-4}	2.6×10^{-6}
5.0	5.0×10^{-4}	8.2×10^{-6}
7.5	1.3×10^{-1}	4.2×10^{-5}

maximum acoustic power leaving the aperture, therefore, must always be limited to

$$P^0_{\max} = I_{\text{peak}} A. \tag{13}$$

This restriction further complicates the range dependent expression of (11). Up to a particular range, R_0, the acoustic power leaving the aperture can be increased to insure that *in situ* intensities reach peak levels. Beyond this range, however, acoustic power levels cannot be increased to provide peak intensities *in situ* because the flux at the transducer surface exceeds guidelines.

The range at which this occurs is simply the point where the product of the focusing gain and the derating equals unity, that is

$$1 = \left[\frac{\lambda^2 R_0^2}{A^2}\right]\left[10^{(0.03\ 2R_0 f/10)}\right]. \tag{14}$$

This expression can be simplified to yield a nonlinear equation for R_0

$$\log_{10} R_0 + \left[\frac{0.03(2R_o f)}{20}\right] - \log_{10}\left[\frac{A}{\lambda}\right] = 0. \tag{15}$$

where again a consistent set of units must be used for proper evaluation. Up to the range satisfying (15), (11) applies. After this range, however, the incident power is limited and the resultant SNR becomes

$$\text{SNR}(R) = \text{SNR}_{\text{inh}}(0) + \Delta - 0.06[2Rf] \tag{16}$$

where

$$\Delta = 20\log_{10}\left[\frac{R_0}{R_{\text{turn-on}}}\right] + 0.03[2R_0 f]. \tag{17}$$

Using these equations, the SNR has been evaluated as a function of range for a typical adult cardiac image. In this computation, a square transducer 15 mm on a side operating with a 40% fractional bandwidth was assumed. In the top panel of Fig. 1 the SNR at 5 MHz for both heart muscle and blood are shown. Similarly, the SNR's for heart muscle and blood at 7.5 MHz are presented in the lower panel of this figure. Clearly, the SNR is well above 0 dB for both heart muscle and blood up to a range of 200 mm at 5 MHz and 150 mm at 7.5 MHz. This means that high-quality adult heart images are possible at 5 MHz up to ranges of 200 mm and at 7.5 MHz up to ranges of 150 mm. These values are well beyond the reach of current imaging systems using impulse excitation. Practical SNR losses due to electromechanical noise figure, focusing errors and individual element radiation patterns, as well as losses due to impulse excitation, dramatically reduce current performance compared to the theoretical bounds of Fig. 1. Efficiently designed imaging systems exploiting the processing gain possible from coded excitation, however, should push routine adult cardiac imaging much closer to these theoretical limits. In the next section, a coded excitation method capable of improving the SNR of current systems by about 15 dB is described.

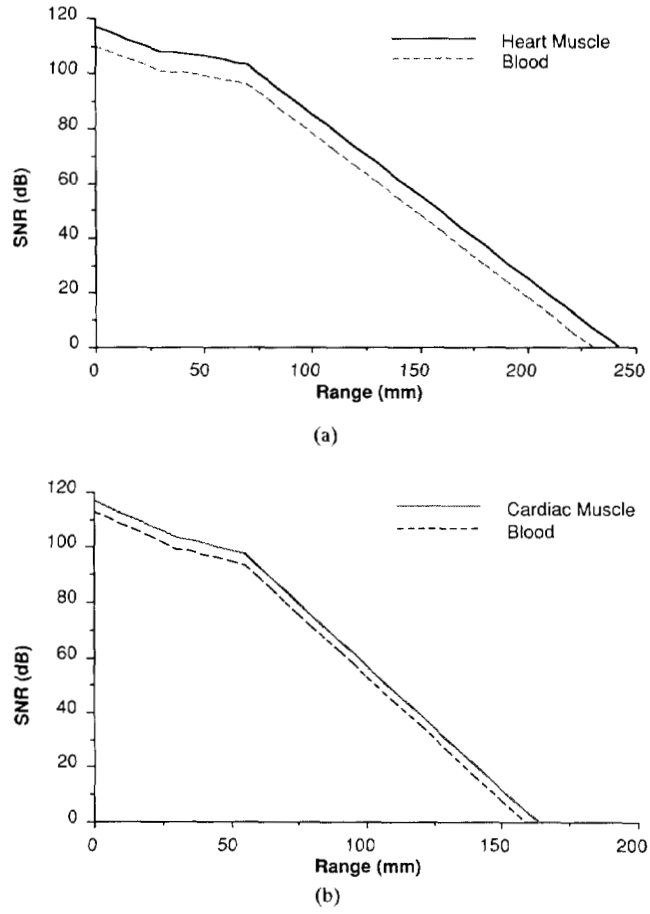

Fig. 1. Calculated theoretical limits of SNR in dB as a function of range for ultrasound images of heart muscle and blood. (a) Adult cardiac imaging where SNR is computed at 5.0 MHz. (b) Adult cardiac imaging where SNR is computed at 7.5 MHz.

II. CODED EXCITATION SYSTEM

The fundamental concept of a coded excitation system is illustrated in Fig. 2. For normal pulse excitation, the axial resolution of a formed beam is determined by the impulse response of the transducer. In a coded system, the excitation pulse extends over a period much longer than the impulse response of the transducer. The excitation sequence, however, includes all frequency components passed by the transducer. Because of this, the received signal can be correlated with a reference waveform to yield a compressed signal with impulse response closely approximating that of the normal pulsed system. The major advantage is that for the same value of instantaneous peak power the SNR of the correlated pulse is improved over that of the normal pulse by a factor close to the time-bandwidth product of the coded excitation sequence [4].

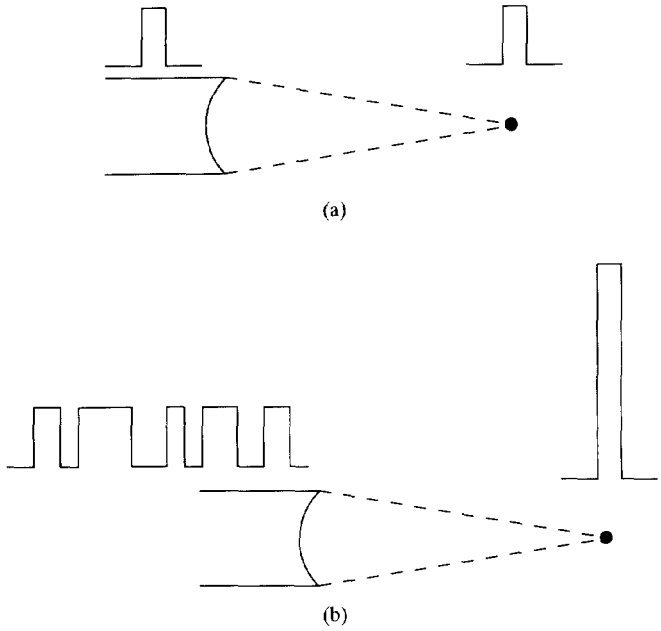

Fig. 2. Graphical illustration of the basic principle of coded excitation. (a) Normal pulse excitation. (b) Coded excitation.

The major disadvantage is that the correlator output possesses range sidelobes not present in the simple pulse system. Consequently, the design of an efficient coded excitation system can be summarized as a trade-off between sidelobe minimization, range resolution and SNR maximization.

The phased-array system proposed here for real-time imaging using efficient coded sequences is illustrated in Fig. 3. The entire system, including both the transmitter and receiver controls on each channel, are synchronized using a single master clock. Each channel in the array is presented with the same excitation code by a master controller. For all cases considered here, the codes consist of single bit streams clocked into the driver at a rate equal to the master clock frequency. To generate a transmitted beam steered in a particular direction and focused to a fixed range, the excitation sequence is delayed independently on each channel using a two step process. First, a coarse delay is generated simply by holding off the bit sequence by an integer count of the master clock period. Second, small variations on this coarse delay are derived by allowing each channel to independently select one of four phases of the master clock to transmit the excitation sequence to the driver for that channel. This two step approach allows long time delays to be generated with an accuracy equal to one fourth the period of the master clock.

The receive signal processing is completely digital, producing a dynamically focused receive beam aligned along the same direction as the transmitted beam. The radio-frequency (RF) echo signal on each channel is separately digitized using the master clock of the system. This digital RF waveform is then demodulated into two data streams referred to as the in-phase (I) and quadrature-phase (Q) components of the baseband representation of the RF signal. The I and Q signals are independently low pass filtered using finite impulse response (FIR) digital filters designed to remove all sum frequency components generated by the demodulator. Coarse time delay of the baseband signal to an accuracy of the master clock period is performed using a FIFO, where the delay is determined by the instantaneous difference between the read and write addresses. The output of the FIFO is then decimated to a rate equal to one eighth of the master clock frequency. This decimation reduces the complexity and speed of all subsequent stages in the digital pipeline. A further time delay accurate to 1/32 of the reference frequency of the demodulator is then performed on the decimated data stream through phase rotation of the baseband signal to a new phase accurate to $2\pi/32$. The magnitude of this phase rotation is changed as a function of range to provide dynamic focus of the receive beam. The coarse time delay and dynamic phase rotation functions are chosen on each channel to correspond to a dynamically focused beam aligned along the same direction as the transmitted beam. Finally, the baseband signals from all array elements are summed (I and Q signals are summed independently) to produce the dynamically focused beam. This processing is described in more detail in [14].

The dynamic receive processing for the digital beam former was originally designed for impulse excitation of the transducer. In this case, the range of the reflected signal is simply defined as $2R = v_s t$, and dynamic focusing is performed assuming that $t = 0$ corresponds to the excitation of the center element of the array. For the coded system depicted in Fig. 3, echoes from multiple ranges are simultaneously received by each array element. Consequently, the proper range for focusing is ambiguous. In this study, dynamic focusing was performed based on the range corresponding to the center of the code. That is, the center of the code is always held in focus. The consequences of performing dynamic focusing in this simple way are discussed later. To recover the final image resulting from the coded excitation, the baseband output of the beam former is correlated with a reference signal at the clock rate of the decimated baseband signal (i.e., $f_{\text{master}}/8$).

Fig. 3 represents a very simple system, primarily because only a single correlator running at baseband rates is needed. Use of a single correlator after the coherent sum, however, means that time varying phase rotation for dynamic focusing, as well as front-end time-gain-control (TGC) variations, are folded into the signal presented to the correlator. To minimize artifacts resulting from a nonstationary gain function, the TGC curve must slowly vary over the duration of the coded pulse and must possess no sharp break points over the entire range of the image. Restriction of the TGC function in this way is not a major problem for the digital beam former described previously, where the analog gain prior to digitization varies monotonically and slowly as a function of range. Indeed, the analog TGC in this system merely insures that the input signal spans a reasonable fraction of the dynamic range of the A/D converter. The output of the digital beam former is normalized prior to correlation to account for this function. Finally, the output of the correlator is subject to a digital TGC prior to entering the display system. This digital function accounts for any sharp, or nonmonotonic, features in the overall system TGC.

Similarly, changes in focusing characteristics over the du-

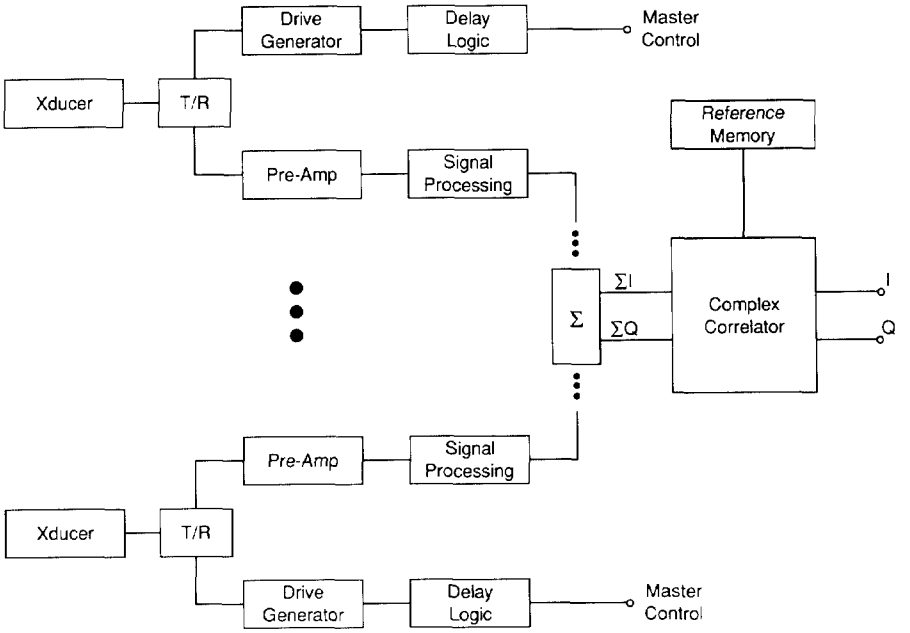

Fig. 3. Block diagram of simple coded excitation system using a single complex correlator acting on the output of the array beam former.

ration of the coded waveform can be minimized by restricting the duration of the code to one focal zone of the receive beam former. A focal zone is defined as the range over which the phase of the outside element differs by less than $|\pi|$ from the focal phase. That is, using the parabolic approximation, the half length of the focal zone ΔR (i.e., $2\Delta R$ is the length of the focal zone) satisfies the relation

$$\frac{ka^2}{2}\left[\frac{1}{R}-\frac{1}{R+\Delta R}\right]=\pi \tag{18}$$

or solving for ΔR:

$$\Delta R \approx 4(f/\text{num})^2\lambda \tag{19}$$

where a is the half width of the aperture, k is the wave number and (f/num) is the instantaneous f/number of the receive lens at any given range. This means that the focal zone for pulse–echo imaging extends over a period Δt,

$$\Delta t=\frac{4\Delta R}{v_s}=\frac{16(f/\text{num})^2}{f}. \tag{20}$$

The excitation pulse cannot exceed this interval. Assuming a minimum f/number of 2, the duration of the coded sequence should be

$$\tau_{\text{code}} < 64/f. \tag{21}$$

For a 40% fractional bandwidth transducer operating in the medical diagnostic frequency range, (21) restricts the time-bandwidth product of coded signals to be about 30.

In general, the single correlator system of Fig. 3 can only be used for sequences with time-bandwidth products less than 50 if significant artifacts due to TGC and dynamic focusing are to be avoided. Since the maximum SNR gain is simply given by the time-bandwidth product, SNR gains of at most 15 dB can be expected for the simple system of Fig. 3. The results of calculations presented in the last section, however, show that at most 20 dB of SNR improvement is theoretically possible. Consequently, short codes used in conjunction with a single correlator at the beam sum should yield SNR gains close to the maximum achievable if range sidelobes can be held to a reasonable level. It should be noted that short codes also have two very practical benefits. First, they need less memory for storage, making implementation much easier. And second, because array imaging systems using all available elements never simultaneously transmit and receive, the "dead" zone at the apex of an image (i.e., at small ranges) is small for short codes.

In this study a number of different binary excitations, including m-sequence and Golay codes, have been examined [4]. Obviously, a code with a δ-function autocorrelation is ideal for imaging. For any practical code, however, the duration is restricted so that a δ-function autocorrelation function can never be obtained, resulting in finite range sidelobes. The range sidelobes for an m-sequence code are constant at a level equal to $1/\sqrt{N}$, where N is the number of points in the code. For the system of Fig. 3, the number N associated with an m-sequence excitation corresponds to the number of independent firings of the array transducer over the duration of the code. This number approximately equals the time-bandwidth product of the system. Consequently, the minimum range sidelobe levels expected from an m-sequence code restricted to a time bandwidth product between 30 and 50 are about 30–35 dB down from the autocorrelation peak. This level is unacceptable for most medical imaging applications.

For the time-bandwidth products permitted by the system of Fig. 3, the peak range sidelobe levels of an individual Golay code are far above those of the m-sequence. Of course, the elegant feature of a Golay pair is that the sum of their autocor-

relations results in a δ-function. This assumes, however, that the object to be imaged is perfectly stationary over the time needed to make independent measurements using both codes of the pair. Because of the very high level of range sidelobes present with the small time-bandwidth products permitted by the system of Fig. 3, this assumption of stationarity becomes very stringent if range sidelobes on the level of -50 dB are to be obtained. For this reason, Golay codes were not investigated further for real-time imaging applications.

Autocorrelation based codes cannot produce the range sidelobes necessary for real-time medical imaging given the restriction on time-bandwidth product imposed by the simple, practical system of Fig. 3. Acceptable range-sidelobe levels can be obtained, however, if matched filtering rather than autocorrelation processing is used. Matched filtering is stable for codes in which the excitation produces a nearly uniform spectrum over the working bandwidth of the transducer. Consequently, a continuous chirp waveform, delivered to each channel of the array with the appropriate time delay accurate to a small fraction of the period of the center frequency of the transducer, represents the ideal excitation. A close approximation to this ideal array system can be obtained using the principle of "pseudochirp" sequences.

The general principle underlying this approach is illustrated in Fig. 4. A binary approximation to a chirp is derived from the expression for a chirp waveform over the bandwidth of the transducer:

$$S(t) = S_0 \cos\left[\left(\omega_0 - \frac{\Delta\omega}{2}\right)t + \frac{\alpha}{2}t^2\right] \qquad (22)$$

where ω_0 is the angular frequency of the carrier, $\Delta\omega$ is the angular bandwidth of the excitation, and α is the slope of the linear chirp. The start of this waveform is synchronized with the master clock and sampled at every clock period over the duration of the chirp. At each sampling point the sign of $S(t)$ is determined. If the sign is positive, then the pseudochirp is set to 1. In contrast, if the signal is either zero or the sign is negative, then the pseudochirp is set to zero. This analysis generates a binary bit stream synchronized to the edges of the master clock. For the example presented in Fig. 4, the clock runs at 40 MHz and a portion of a pseudochirp sequence centered at 5 MHz is shown. The excitation sequence of Fig. 4 is then convolved with the transducer response to produce the coded waveform. Because of truncation effects resulting from representing a continuous waveform by a two-level signal, the spectrum of the code is not smooth over the passband of the transducer. To illustrate this, we investigate the response of the baseband receiver to a sequence of the type shown in Fig. 4.

In Fig. 5 we present the response of the digital baseband receiver described previously operating at a reference frequency of 5 MHz to a 512-point, 40-MHz-clocked pseudochirp code centered at 5 MHz with a bandwidth of 2 MHz (i.e., 40% fractional bandwidth, 12.8-μs code representing a time-bandwidth product of approximately 25). The Fourier transform of this code is presented in Fig. 6, where dc represents the 5 MHz component of the actual excitation waveform. The binary excitation approximates the general spectral characteristics of a chirp. The detailed spectral response, however, deviates from

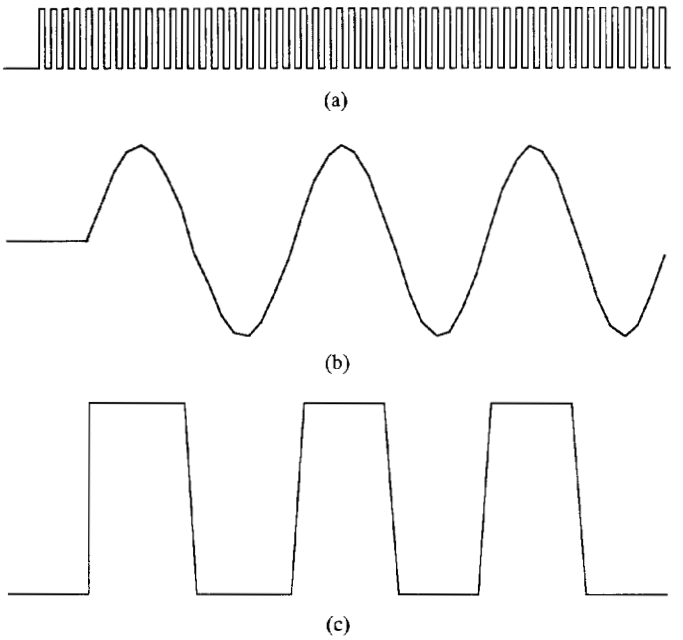

Fig. 4. Illustration of a binary "pseudochirp" excitation function. (a) Master clock. (b) Chirp. (c) Pseudochirp.

the simple rectangular spectrum of a pure chirp. Nevertheless, because there are no singularities over the passband, this spectrum can be inverted to derive matched filter coefficients.

Generally, the spectrum must be inverted with care to insure that no ringing occurs in the final correlator output. In this study, the following inversion algorithm was used

$$\begin{aligned} M(f) &= \frac{|H(f)|_{\max}}{H(f)} && \text{for } |\mathrm{H(f)}| \geq \mathrm{s}|\mathrm{H(f)}|_{\max} \\ &= 0 && \text{for } |H(f)| < s|H(f)|_{\max} \end{aligned} \qquad (23)$$

where $H(f)$ is the complex excitation spectrum, $M(f)$ is the complex matched filter spectrum, $|H(f)|_{\max}$ is the maximum value of the magnitude of the excitation spectrum over the passband and s is a scale factor based on the magnitude of oscillations in the passband. This scale factor insures that all frequencies within the primary passband contribute to the inverse filter and all frequencies outside this band are ignored. The matched filter defined by (23) is then inverse Fourier transformed to obtain the complex coefficients for the correlator reference. In Fig. 7 the output of the correlator for the signal of Fig. 5 is presented using a matched filter with a scale factor of -6 dB (i.e., s =0.5). A raised cosine window function was multiplied with the reference waveform to reduce range sidelobes at the slight expense of mainlobe width. Obviously, a tight mainlobe is produced. Rather high sidelobes, however, are also produced. Indeed, the level of sidelobes shown in Fig. 7 is unacceptable for medical imaging.

In normal binary correlation systems, the duration of the matched filter equals that of the excitation function. If the filter is derived using Fourier methods, as described previously, then the resultant reference waveform represents the matched filter response assuming a circular correlation. Of course, in the actual imaging system a linear correlation is performed, resulting in rather high sidelobe levels as illustrated in Fig.

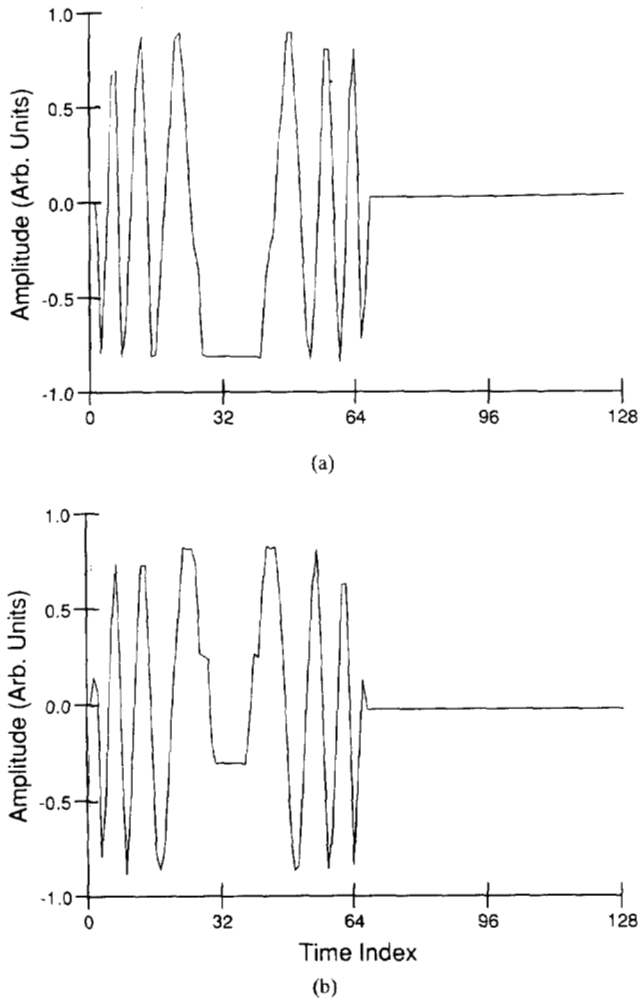

Fig. 5. Complex (top panel in-phase signal, lower panel quadrature phase signal) output of digital baseband system for pseudochirp input. (a) I channel. (b) Q channel.

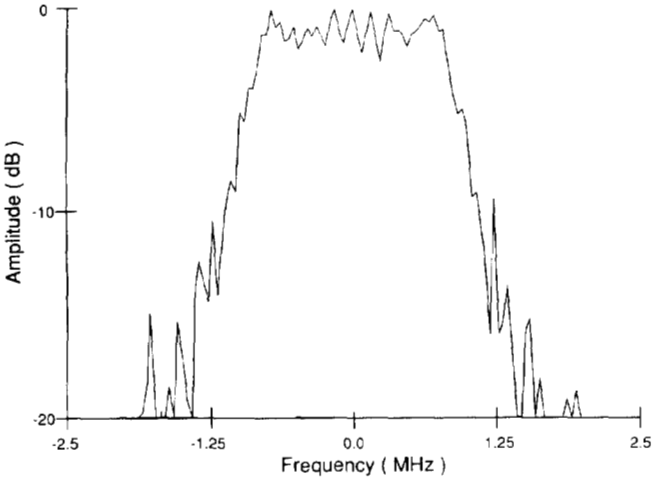

Fig. 6. Baseband excitation spectrum of the pseudochirp of Fig. 5.

7. To improve sidelobe level performance of the proposed coded excitation system, a slight modification to the correlator reference must be made to overcome this effect.

Equalization filtering, where the duration of the matched filter is extended, can be used to markedly reduce the range

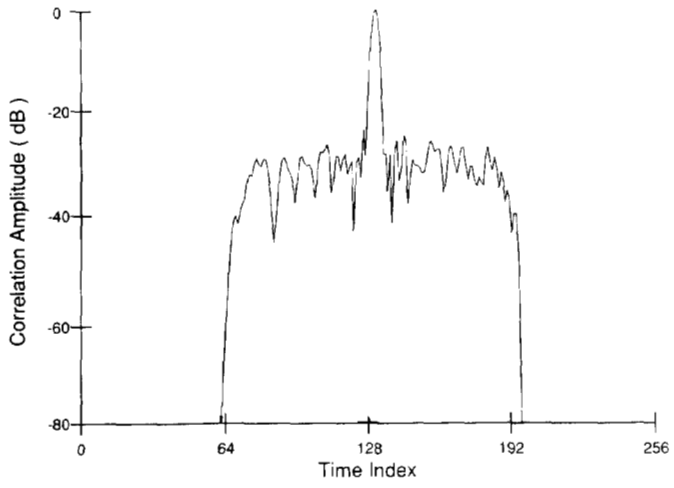

Fig. 7. Output of complex baseband correlator using conventional matched filter for pseudochirp of Fig. 5. N-point correlation. Scale= -6 dB.

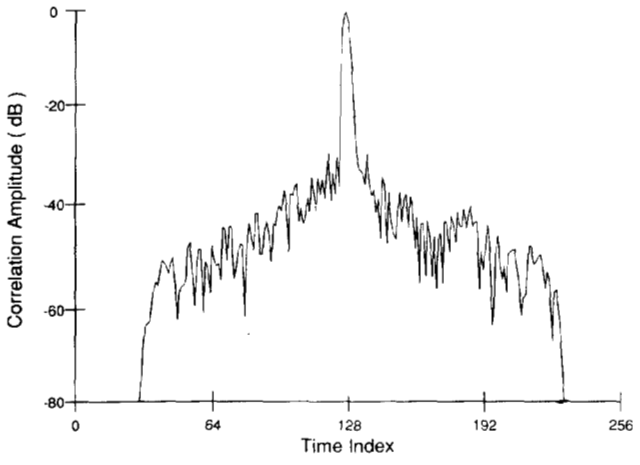

Fig. 8. Output of complex baseband correlator using 2:1 equalization filter for pseudochirp of Fig. 5. Central $2N$ points of $4N$ reference. Scale $=-6$ dB.

sidelobes produced by the simple Fourier method described previously [15]. Using this approach, the length of the matched filter impulse response may exceed the duration of the excitation waveform. This is done to reduce the peak height of range sidelobes at the expense of sidelobe duration. To illustrate the performance of this method, a different matched filter was derived from the waveform of Fig. 5 using the same scale factor of -6 dB but extending the duration by a factor of 2. The filter coefficients were obtained by zero padding a sampled version of Fig. 5 to 4 times the length of the excitation ($4N$), Fourier transforming the resulting signal, deriving the matched filter using (22), inverse Fourier transforming $M(f)$, retaining only the central half of the final time domain waveform ($2N$) and multiplying the final waveform with a raised cosine window function extending over $2N$ points. If this waveform is used as the correlator reference for the signal of Fig. 5, then the output of Fig. 8 results. Clearly, average range sidelobe levels have been greatly reduced at the price of extending the duration of these sidelobes by a factor of 1.5.

Usually, filter coefficients can be selected in an optimal fashion by defining a desired correlator output based on a

reasonable average sidelobe level and minimizing the weighted mean square error between the actual output and the desired output with respect to the filter coefficients of the extended waveform [15]. In this study, optimal filter coefficients derived in this way were not used. Nevertheless, a comparison of the results presented in Figs. 7 and 8 demonstrates the general utility of the equalization approach, where the duration of the correlator reference is extended.

III. Experimental Results

To test the methods described previously, measurements were obtained on an experimental system performing the processing of Fig. 3. A bit serial data generator clocked at 17.76 MHz was used to deliver the same coded sequence to all elements of a 64 channel, 3.33 MHz, 40% fractional bandwidth phased-array transducer. The same 17.76 MHz clock was used to sample the A/D converter of the digital receive beam former. Thus, the coded transmit pulse was always phase locked to the receive sampler. The excitation code was 256 points long, representing about a 14.4 μs pulse. Because of frequency translation and decimation in the digital receive beam former (2.22 MHz output clock), this pulse reduces to a 32 point code at the baseband frequency. Full dynamic focusing on receive, as described previously, was maintained at the center of the code. Transmitter time delays, accurate to one fourth the period of the 17.76 MHz master clock, were applied to form a fixed transmit focus at a depth of 80 mm. All measurements and images shown in the following used a conventional sector scan format, where a full 90° sector was scanned with 128 independent beams. Each beam of the image corresponds to an independent firing of the transducer (i.e., parallel beams are not formed on a given firing).

All measurements reported have used a pseudochirp sequence. The spectrum of this chirp over a 2.22-MHz band centered at 3.33 MHz is presented in Fig. 9 (bottom panel) along with the spectrum of the insonifying transducer (top panel). Using this excitation spectrum, a 64 point long (at baseband rates) matched filter was designed using the equalization approach described previously. Finally, by multiplying the two spectra of Fig. 9, the spectrum of the actual ultrasound pulse is produced, as illustrated in Fig. 10.

Images of a set of five wires immersed in water (center wire at a range of 80 mm) are presented in Fig. 11. The display scale for this image, and all subsequent images, is purely logarithmic over a dynamic range of 40 dB. The top left image was obtained with a standard impulse excitation, whereas the top right image used a chirp code without any correlation after the coherent summation. In contrast, the lower left image was made with the correlator in place. A quick comparison between the two images on the left side shows that no significant artifacts have been generated by the coded excitation system. A more quantitative demonstration of the quality of the correlation system is presented in Fig. 12. This figure shows the A-Scan corresponding to the central beam of the two left hand images of Fig. 11, where the top panel is the response of the coded system and the lower panel is the response of the conventional imaging system. Artifacts produced by the coded system are on the order of 45–50 dB down from the primary signal. Since these artifacts extend over a very short range (i.e., about ±8 mm), this level of range sidelobe level rejection should be adequate for many imaging applications.

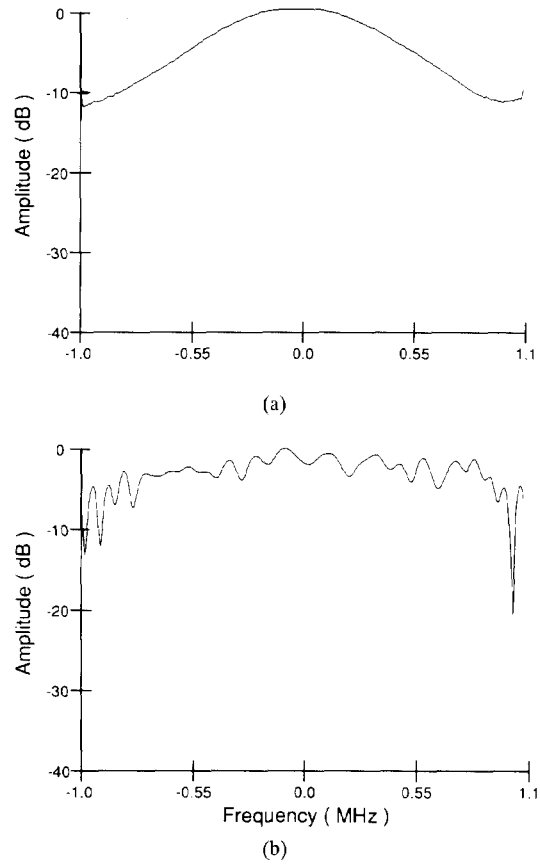

Fig. 9. Baseband spectrum of array transducer used in experiments (a) and baseband spectrum of pseudochirp used to drive transducer (b).

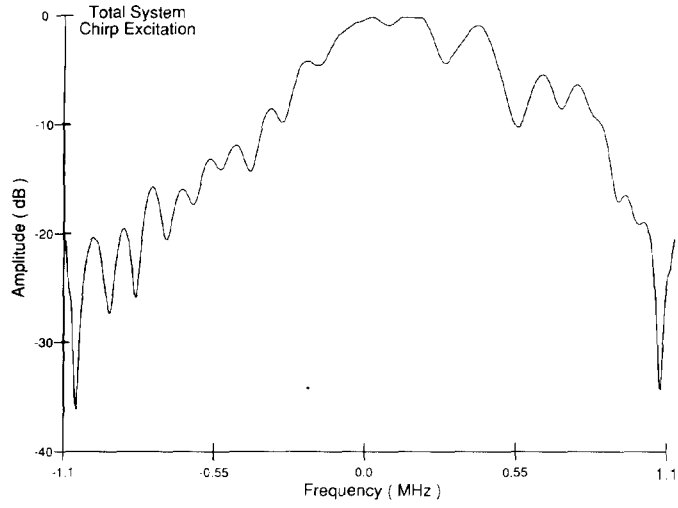

Fig. 10. Baseband spectrum of excitation created by driving transducer with the pseudochirp spectrum of Fig. 9.

Finally, images of a standard resolution phantom were made with the same chirp code.[1] In Fig. 13, these images are

[1]The phantom used for imaging experiments is model #84–317 from Radiation Measurements Inc.

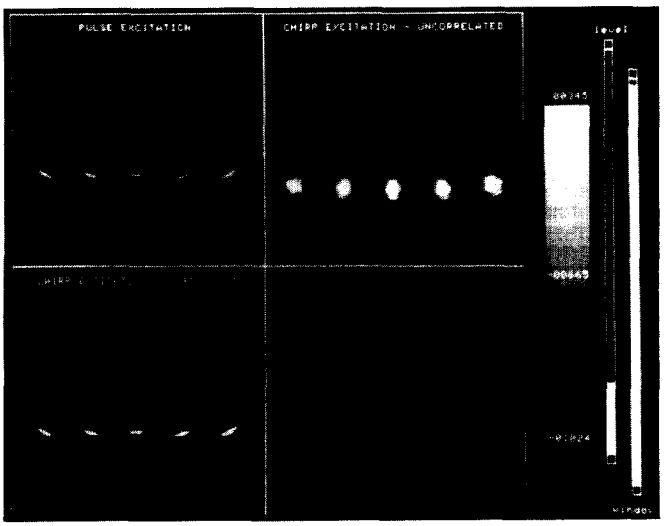

Fig. 11. Images of wire targets in water demonstrating correlation processing. All figures are displayed using a purely logarithmic gray-scale distributed over a 40-dB dynamic range. The top left image is obtained with conventional pulse excitation, top right image acquired with pseudochirp excitation without subsequent correlation processing, and lower left image is the result of correlation processing the pseudochirp waveform using a 2:1 equalization filter.

compared to images of the same phantom made with conventional impulse excitation. The left hand images correspond to impulse excitation and the right-hand images correspond to chirp excitations, where the upper images are displayed to a range of 100 mm and the lower images to a range of 175 mm. All images were made with the same peak power, but the average power in the chirp exceeded the impulse excitation by over 13 dB. For the level of attenuation present in this phantom, the processing gain should result in additional penetration of 40–50 mm. A comparison of the upper images demonstrates that the image quality, including spatial resolution, texture magnitude and frequency and artifact level, is virtually identical for the two methods. An inspection of the lower images, however, demonstrates the enhanced penetrating power of the coded system.

IV. Conclusion

Based on calculations of the intrinsic SNR in medical ultrasound imaging, it is clear that current 2-D imagers are working far below theoretical limits. Indeed, if both peak and average acoustic intensities are simultaneously kept at maximum accepted limits, then there is a factor of 15- to 20-dB improvement possible in the SNR of current systems. Using coded excitation, it is possible to realize most of this potential 15–20 dB improvement in SNR. If such improvements can be produced on actual imagers without adversely affecting image quality, then the performance of these systems will push theoretical bounds, permitting routine imaging at higher frequencies. In this paper, a simple system based on the principles of pseudochirp excitation and equalization filtering has been examined. Equalization filtering can be used to reduce the average sidelobe levels of short codes by increasing the size, and hence the complexity, of the correlator. The overall

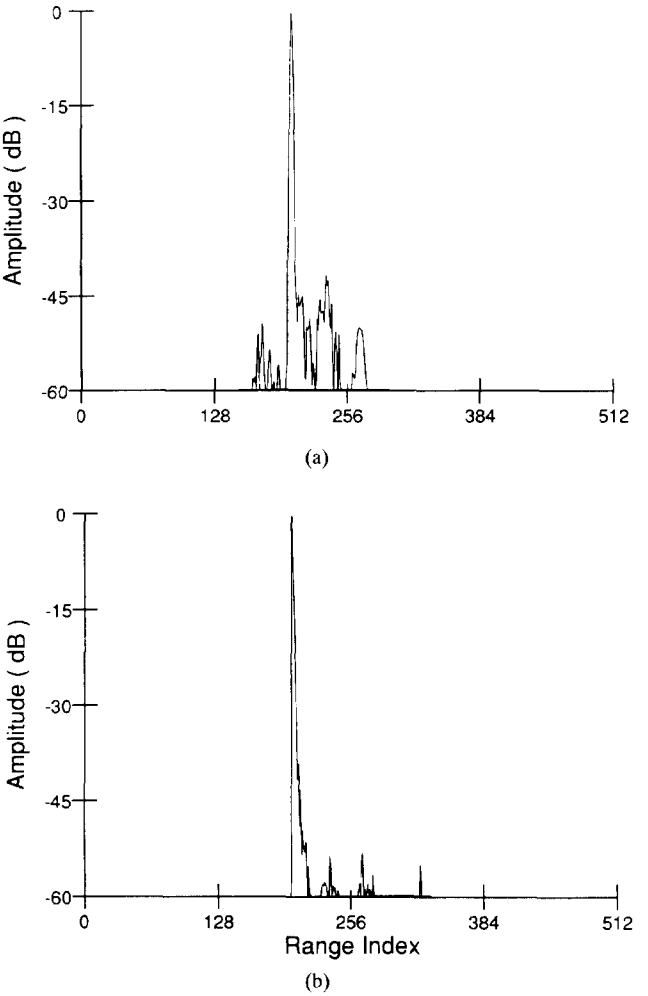

Fig. 12. A-scan (beam 64) of the central beam of the two left hand images of Fig. 11. (a) A-scan for chirp excitation with correlation processing. (b) A-scan for conventional pulse excitation.

Fig. 13. Images of an AIUM resolution phantom comparing conventional pulse excitation (left side) to chirp excitation with correlation processing (right side).

performance improvement obtained by equalization is directly related to the length of the matched filter impulse response.

Both the extent of these sidelobes, and the cost of the elongated correlator, must be traded-off with average sidelobe levels in designing a practical system.

The system presented in this paper produces only a single image for each firing of the array. It is possible to conceive of extending this system to obtain multiple transmit beams on a given firing using an orthogonal coding approach. Because of the spatially continuous nature of scattering in the body, however, the degree of orthogonality needed is quite high to insure artifact free imaging [16]. Given the time bandwidth products available to real-time phased-array imagers, it does not seem possible that the simple system presented in this paper can be easily extended to handle multiple simultaneous transmit beam formation.

Possible further improvements in performance of the system presented here can be obtained through elongation of the basic codes. The performance of long codes, however, can be dramatically reduced due to dynamic focusing and TGC functions in the front-end of a phased-array receiver. The dynamic receiver must focus at the *center* of the excitation pulse at every depth so that the two ends of the pulse will be out of focus to the same degree. As shown previously, by choosing the duration of the pulse to be less than the depth of field at the minimum f/number of the aperture, dynamic focusing should not cause major complications. If the pulse is extended beyond this length, then significant artifacts can be produced. Also, if the pulse is greatly extended, then restrictions on the TGC function for the digital beam former cannot be maintained without introducing significant digital noise into the system as a result of the finite number of bits in the A/D converter

To extend the duration of codes over a single focal zone of the array, individual correlators and digital TGC's are needed *per channel* so that gain normalization and decorrelation are performed before beam forming. In this way, decorrelation is performed on a properly normalized waveform of arbitrary temporal extent to produce a short pulse on each channel in the array. Dynamic focusing can be applied to the resultant pulse waveform without any ambiguity. This is a major price to pay, however, especially since an increase in pulse length by a factor of 2 only reduces average range sidelobes by a factor of 6 dB. Consequently, the simple single correlator system presented here represents a reasonable approach to coded imaging.

In this study, a very straightforward method was used to derive coefficients of the elongated matched filter. Clearly, optimal design of these coefficients must be studied. In particular, a minimum mean square error method should be compared to the simple method presented here to quantitate possible further improvements. In a minimum mean square error approach, the error metric is defined as

$$\varepsilon = \sum_{i=1}^{N} W_i \left[D_i - \sum_{j=1}^{M} \tilde{F}_j \tilde{S}_{i+j} \right]^2 \qquad (24)$$

where N is the number of points over which the correlator output is sampled, M is the number of points in the matched filter response, D_i are the desired outputs of the matched filter, $\tilde{F}_i$ are the complex matched filter coefficients, $\tilde{S}_i$ represents the complex excitation signal and W_i is a weight. The number of points N is chosen to be the sum of the length of the excitation signal and the length of the matched filter response (e.g., for a 2:1 equalization filter $N = M + 2M = 3M$). The desired output and weighting terms are chosen assuming an average range sidelobe level. Based on (24), the error metric is minimized with respect to the complex filter coefficients to obtain optimal values in the least squares sense [15].

Finally, experimental results have been presented demonstrating that a coded excitation system can generate artifact free images with processing gains approaching theoretical limits. As noted in the introduction, processing gains between 15 and 20 dB are possible. The system presented here is capable of processing gains approaching 15 dB over the diagnostic range of frequencies, a level approaching theoretical bounds and representing a significant improvement in penetration. With this level of improved penetration, basic operating frequencies can be increased. For example, routine adult cardiac imaging is performed primarily at 3.5 MHz. Using the system presented here, the same images can be acquired at 5.0 MHz. To insure range-sidelobe levels appropriate for high-quality diagnostic imaging, the output of the mainlobe of the matched filter may be extended by as much as 50% compared to the impulse response of the transducer. Nevertheless, such a loss in axial resolution is more than compensated by the higher operating frequency. For example, if the same size transducer aperture is used at both 5.0 MHz and 3.5 MHz, then at 5 MHz a 3-D voxel is only half the size of the voxel at 3.5 MHz even assuming that the fractional bandwidth of the coded 5.0 MHz system is reduced by 50% compared to a simple pulsed 3.5 MHz system. Because of this, and the simplicity of the excitation and correlation electronics, the coded excitation system presented here appears to be an attractive approach to increasing the spatial resolution of real-time ultrasonic imaging systems.

ACKNOWLEDGMENT

The author would like to thank his pals at the University of Michigan, Emad Ebbini and Charles Cain, for helpful comments on the manuscript. He would also like to thank Jerry Tiemann of GE-CRD for useful discussions at the beginning of this work on equalization filtering. Also, helpful comments by the referees of the original manuscript are gratefully acknowledged.

REFERENCES

[1] AIUM-NEMA, "Safety standard for diagnostic ultrasound equipment," *J. Ultrasound Med.*, vol. 2, p. 51, 1983.
[2] Eli Brookner, "Phased array radars," *Scientific Amer.* 252, no. 2, p. 94, 1985.
[3] V. L. Newhouse, D. Cathignol and J. Y. Chapelon, "Introduction to ultrasonic pseudo-random code systems," in *Progress in Medical Imaging*, V. L. Newhouse, Ed. New York: Springer-Verlag, 1988, pp. 215–226.
[4] J. Y. Chapelon, "Pseudo-random correlation imaging and system characterization," in *Progress in Medical Imaging*, V. L. Newhouse, Ed. New York: Springer-Verlag, 1988, pp. 227–246.
[5] D. Cathignol, "Pseudo-Random correlation flow measurements," in *Progress in Medical Imaging*, V. L. Newhouse, Ed. New York: Springer-Verlag, 1988, pp. 247–279.

[6] V. L. Newhouse, "Pseudo-random characterization of time-varying media," in *Progress in Medical Imaging*, V. L. Newhouse, Ed. New York: Springer-Verlag, 1988, pp. 281–290.
[7] V. L. Newhouse, "Pseudo-random multimode operation," in *Progress in Medical Imaging*, V. L. Newhouse Ed. New York: Springer-Verlag, 1988, pp. 291–301.
[8] Y. Takeuchi, "An investigation of a spread energy method for medical ultrasound systems." *Ultrason.* vol. 17, 175, 1979.
[9] C. R. Meyer, "Preliminary results on a system for wideband reflection-mode ultrasonic attenuation imaging," *IEEE Trans. Sonics Ultrason.* vol. SU-29, 12, 1982.
[10] S. Kiryu, T. Moriya, M. Yosizawa, and T. Fuse, "FM chirp pulse compression system for ultrasono-tomography," *Proc. 1984 Int. Symp. Noise and Clutter Rejection in Radars and Imaging Sensors*, T. Musha, T. Suzuki, and H. Ogura, Eds., 176, 1984.
[11] R. A. Sigelmann and J. M. Reid, "Analysis and measurement of ultrasound backscattering from an ensemble of scatterers excited by sine-wave bursts," *J. Acoust. Soc. Amer.*, vol. 53, p. 1351, 1973.
[12] M. O'Donnell, J. W. Mimbs and J. G. Miller, "Relationship between collagen and ultrasonic backscatter in myocardial tissue," *J. Acoust. Soc. Amer.* vol. 69, p. 580, 1981.
[13] K. K. Shung, R. A. Sigelmann, and J. M. Reid, "The scattering of ultrasound by blood," *IEEE Trans. Biomed. Eng.*, vol. BME-23, p. 460, 1976.
[14] M. O'Donnell, W. E. Engeler, J. T. Pedicone, A. M. Itani, S. E. Noujaim, R. J. Dunki-Jacobs, W. M. Leue, C. L. Chalek, L. S. Smith, J. E. Piel, R. L. Harris, K. B. Welles, and W. L. Hinrichs, "Real-time phased array imaging using digital beam forming and autonomous channel control," *Proc. 1990 IEEE Ultrason. Symp.*, 1990, p. 1499.
[15] K. Pahlavan, "Signal processing in telecommunications," in *Signal Processing Handbook*, C. H. Chen Ed. New York: Marcel Dekker, 1988, pp. 698–713.
[16] B. B. Lee and E. S. Fergason, "Pseudo-random codes for single mode operation in ultrasonic imaging systems," School of Electrical Engineering, Purdue University, West Lafayette, IN, Tech. Report TR-EE 85–10, May 1985.

Matthew O'Donnell (M'79–SM'84) received the B.S. and Ph.D. degrees in physics in 1972 and 1976, respectively, from the University of Notre Dame, Notre Dame, IN.

He was a postdoctoral fellow in the Physics Department of Washington University, St. Louis, MO, where he worked on applications of ultrasonics to medicine and nondestructive testing. He subsequently held a joint appointment as a Senior Research Associate in the Physics Department and a Research Instructor of Medicine in the Department of Medicine at Washington University. In 1980, he joined the General Electric Corporate Research and Development in Schenectady, NY, where he worked on medical electronics, including NMR and ultrasound imaging systems. During the 1984–1985 academic year, he was a Visiting Fellow in the Department of Electrical Engineering at Yale University, New Haven, CT, where he investigated automated image analysis systems. More recently, he has worked on the application of advanced VLSI circuits to medical imaging systems. In 1990, he joined the Electrical Engineering and Computer Science Department of the University of Michigan, Ann Arbor, where he is a Professor.

Dr. O'Donnell is a member of Sigma Xi and the American Physical Society. He has authored and co-authored more than 60 articles for archival publications (including two that received Best Paper awards), papers that were presented at numerous national meetings, and 31 patent applications (23 of which have been issued patents).